ACS Sustainable Chemistry & Engineering

Research Article

pubs.acs.org/journal/ascecg

Porous NiO/C Nanocomposites as Electrode Material for Electrochemical Supercapacitors

Subbukalai Vijayakumar, Sadayappan Nagamuthu, and Gopalan Muralidharan*

Department of Physics, Gandhigram Rural Institute, Deemed University, Gandhigram, Tamilnadu, India

Supporting Information

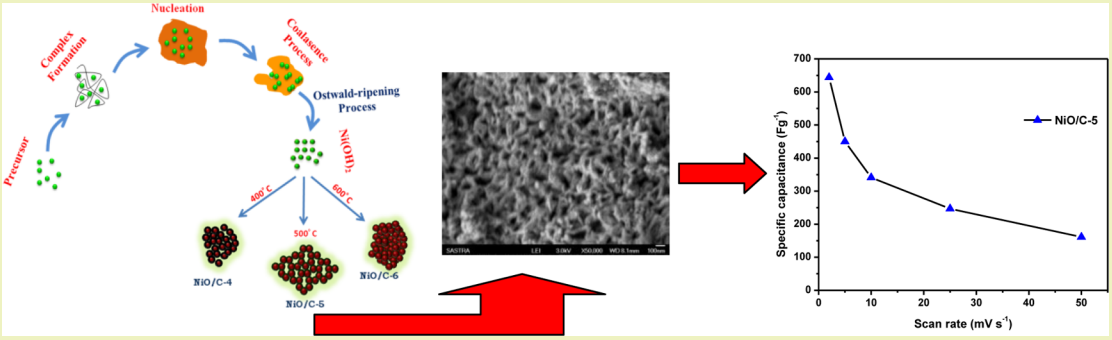

ABSTRACT: NiO/C nanocomposites were synthesized at different calcination temperatures using starch as the stabilizing agent. The NiO/C nanocomposites were characterized by thermogravimetric analysis (TGA), X-ray diffraction (XRD), Fourier transform infrared spectroscopy (FTIR), field emission scanning electron microscopy (FESEM), and transmission electron microscopy (TEM). The samples calcined at 500 °C exhibit a highly porous nature. Electrochemical investigations of NiO/C were carried out using cyclic voltammetry, chronopotentiometry, and electrochemical impedance spectroscopy. NiO/C-5 shows excellent electrochemical performance compared to NiO/C-4 and NiO/C-6. The NiO/C-5 electrode exhibits a specific capacitance value of 644 F g^{-1} at a scan rate of 2 mV s^{-1}. The charge transfer resistance is 0.59 Ω for the NiO/C-5 electrode. This NiO/C-5 appears to be a promising electrode material for supercapacitor applications.

KEYWORDS: *Nickel oxide, Nanocomposites, Supercapacitor*

INTRODUCTION

Nanomaterials have been attracting great interest due to their potential use in applications such as supercapacitors,[1] batteries,[2] sensors,[3] and solar cells.[4] Nanoelectrodes have several advantages in electrochemical technology, such as higher charge−discharge rates due to higher surface to volume ratio and shorter path length for electronic transport and ion transport.[5] In electrochemical technology, supercapacitors receive a special place because they bridge the gap between batteries and conventional capacitors and result in specific capacitance from 6 to 9 orders of magnitude larger than conventional capacitors.[6,7] In addition, their ability to deliver stored energy more rapidly than batteries and their higher power density and long cycle life make supercapacitors a complement or replacement for batteries in portable electronic devices, hybrid electric vehicles, and long time constant circuits.[8] Supercapacitors store charges using reversible adsorption of ions at the electrode and electrolyte interface (electric double layer capacitor (EDLC)) or redox reaction on the surface of the electrode (redox supercapacitors).[9] Pseudocapacitors exhibit higher energy density than EDLCs. Metal oxides such as RuO_2, MnO_2, NiO, Co_3O_4, metal sulfides, and conducting polymers[10−15] have been used as pseudocapacitor electrode materials. Among these materials, RuO_2 exhibits higher specific capacitance in an acidic electrolyte. However, the toxicity and low abundance have necessitated the need to develop other inexpensive materials of comparable performance. NiO is a likely replacement for RuO_2 due to its high theoretical specific capacitance, high chemical and thermal stability, and low cost.[16]

Because pseudocapacitance is an interfacial phenomenon related to the surface morphology of the electroactive material, it is expected that the porous structure of a material enhances the electrochemical properties by shortening the diffusion path and by providing a large active surface area for ions. This porous structure not only increases the mass transport of the ions but also maintains the structure stable during the continuous cycling process.[17] Xia et al.,[18] reported the porous NiO maintains its morphology even after 4000 continuous cycles and remains unaffected by the damage caused by volume expansion during the continuous cycling process. Even though thin film morphology shows higher capacitance, powders are desirable due to low volumetric density of thin films.

Carbon coating on nickel oxide enhances the supercapacitor performance of the electrode material. Fan et al.[19] recently

Received: January 21, 2013
Published: June 12, 2013

   dx.doi.org/10.1021/sc400152r | ACS Sustainable Chem. Eng. 2013, 1, 1110−1118

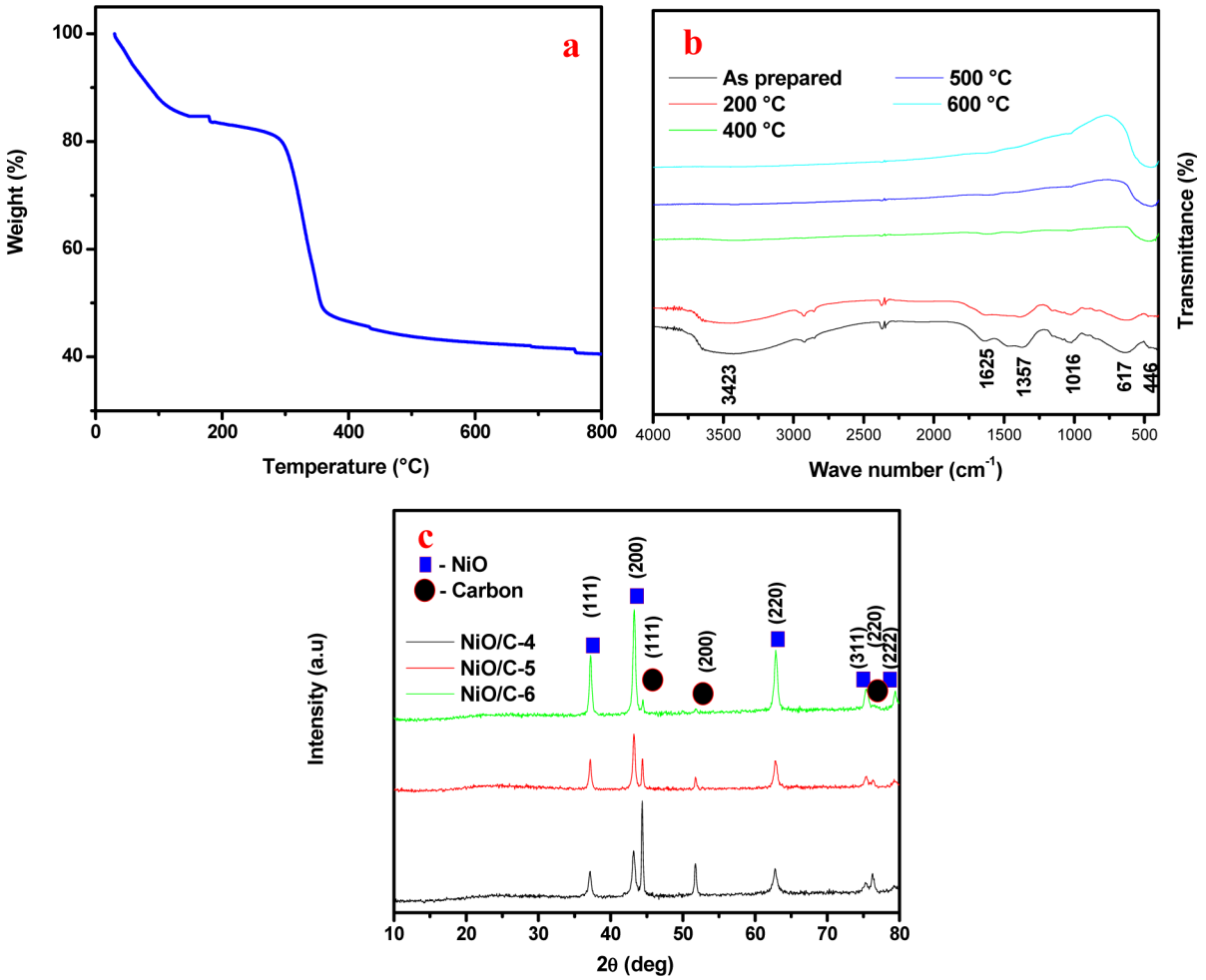

Figure 1. (a) TGA of uncalcined sample. (b) FTIR spectrum of samples calcined at different temperatures. (c) XRD patterns of NiO/C samples.

reported increased supercapacitor behavior of carbon encapsulated nickel oxide. They further attributed the improved performance to the encapsulation. Huang et al.[20] also reported the net-structured NiO-C nanocomposites to exhibit excellent electrochemical properties.

In this paper, we report the green synthesis of nickel oxide/carbon (NiO/C) nanocomposites using starch and dextrose as the carbon sources. A possible mechanism for the formation of porous NiO/C is proposed. Influence of calcination temperature on the morphology and carbon coating has been discussed. The electrochemical performance of NiO/C nanocomposites prepared at calcination temperatures of 400, 500, and 600 °C as a supercapacitor electrode material in 2.0 M KOH electrolyte has been reported and discussed.

EXPERIMENTAL METHODS

Material Synthesis. Analytical grade nickel nitrate hexahydrate (Sigma Aldrich), dextrose (Merck), and starch (Merck) were used. In a typical preparation process, 0.1368 g of soluble starch was dissolved in 400 mL of water, followed by the addition of 40 mL of 0.1 M nickel nitrate hexahydrate and 60 mL of 0.1 M dextrose with continuous stirring at room temperature. Subsequently, the pH of the solution was raised slowly to 10 by the drop by drop addition of an aqueous solution of ammonia. The resultant solution was continuously stirred for 3 h. Finally, the mixture was allowed to precipitate at room temperature. The colloidal precipitate was thrice washed in water. The precipitate was again washed in a mixture of water and ethanol. After centrifugation, the precipitate was finally washed in absolute ethanol. After this wash, the precipitate was dried in an atmosphere of air at 60 °C for 24 h to get the nanopowder. Finally, the as-prepared powders were converted into nickel oxide/carbon (NiO/C) nanocomposites by calcining at 400, 500, and 600 °C for 2 h in air. The samples prepared under various calcining temperatures are denoted as NiO/C-4, NiO/C-5, and NiO/C-6. For example, NiO/C-4 denotes the nanocomposites calcined at 400 °C.

Material Characterization. Thermogravimetric analysis (TGA) was performed from room temperature to 800 °C using EXSTAR6200 TGA from SII Nanotechnology, Inc., Japan, at a heating rate of 20 °C per minute. FTIR spectra were recorded using a Perkin-Elmer SPECTRUM BX II spectrometer. The X-ray diffraction (XRD) measurements were made from 10 to 80 °C using a Panalytical XPERT−PRO X-ray diffractometer with Cu Kα (1.5406 Å) radiation to determine the phase and purity of the prepared samples. The grain sizes of the NiO/C samples were estimated using the Debye−Scherrer equation. The surface morphology of the nanocomposites was studied using a field emission scanning electron microscope (FESEM) JEOL JSM 6701F instrument. Energy dispersive spectra (EDS) were recorded using Bruker Quantax 200 AS instrument. The TEM measurement was made using Hitachi H-7100 KVA. The N_2 adsorption−desorption measurement was carried out on a Micrometrics ASAP 2020 analyzer using the Brunauer−Emmett−Teller (BET) gas adsorption method.

Electrode Preparation and Electrochemical Measurements. The working electrodes were fabricated by mixing 80 wt % of NiO/C with 15 wt % of activated carbon using a mortar and pestle. To this mixture, 5 wt % of polytetrafluoro-ethylene (PTFE) was added with the addition of ethanol to form a slurry. The slurry was coated on a graphite sheet of 1 cm^2 area. Finally, the electrode was dried at 80 °C

dx.doi.org/10.1021/sc400152r | ACS Sustainable Chem. Eng. 2013, 1, 1110−1118

for 6 h. The loading mass of the active material was 0.8 mg. The electrochemical performance was analyzed using a CHI 660 D Electrochemical workstation. The electrochemical measurements were carried out using three electrode cell configurations with NiO/C as the working electrode, platinum as the counter electrode,and Ag/AgCl as the reference electrode. The measurements were performed using 2.0 M KOH as the electrolyte. The cyclic voltammetry (CV) measurements were performed at different scan rates, 2, 5, 10, 25, and 50 mV s^{-1}, in a potential window from 0 to 0.5 V. The charge−discharge measurements were performed at different current densities in a potential window from −0.05 to 0.45 V. The electrochemical impedance measurements were carried out between 0.01 Hz and 100 kHz with an AC amplitude of 5 mV and bias potential of 0.4 V.

RESULTS AND DISCUSSIONS

Thermogravimetry and Structural Studies. The thermal and structural studies give the details of phase changes and possible decomposition of the sample and phase and purity of the NiO/C composites. FESEM studies yield information on the influence of temperature on the morphology of the material. To understand the changes that occur in the nanocomposites, thermal studies were carried out from room temperature (RT) to 800 °C at a heating rate of 20 °C/min. Figure 1a shows the thermogravimetric curve (TGA) of NiO/C. A three-step weight loss, RT to 200 °C, 200−360 °C, and 360−800 °C could be observed. In order to discuss the weight loss in TGA, FTIR spectra have been recorded for the uncalcined sample and for samples treated at 200, 400, 500, and 600 °C in an atmosphere of air. Figure 1b shows the FTIR spectra of as-prepared sample and samples calcined at 200, 400, 500, and 600 °C. The broad band at 3423 cm^{-1} is attributed to the O−H stretching vibration of interlayer H_2 molecules.[21] The sharp absorption at 1625 cm^{-1} is assigned to the vibration of water molecules.[22] The sharp peak at 1357 cm^{-1} is due to interlayer NO_3^- molecule.[22] This may due to the presence of a small quantity of nitrate trapped in the nanoparticles during the formation process. The narrow band at 1016 cm^{-1} is assigned to the vibration of the C−O bond.[21] The band centered at 617 cm^{-1} is attributed to the δNi−OH vibrations.[22] The band at 446 cm^{-1} corresponds to the Ni−O.[21]

The uncalcined product contains both adsorbed and intercalated water molecules. The structural water present in the uncalcined product is removed in a multistep process at different temperatures. The first weight loss of about 17% has occurred up to 200 °C. It corresponds to removal of intercalated and adsorbed water molecules.[23] FTIR also supports the weight loss due to the water molecules as evidenced by a large decrease in the strength of the band at 3423 cm^{-1}. The second weight loss of ∼30% occurring between 300 and 360 °C, corresponds to the dehydration of $Ni(OH)_2$ and decomposition of carbonaceous materials.[24] The FTIR sample calcined at 200 and 400 °C confirms the conversion of $Ni(OH)_2$ to NiO between 200 and 360 °C. The third weight loss starts from 360 to 800 °C. Above 360 °C, weight loss continues, but it is small. The FTIR spectra for samples treated at temperature above 400 °C do not show any band other than Ni−O. The carbon starts to burn off while increasing the temperature.

The XRD patterns of NiO/C-4, NiO/C-5, and NiO/C-6 are shown in Figure 1c. In all the three cases, the formation of NiO in crystalline phase could be observed, along with the same diffraction peaks corresponding to carbon. It is observed that the carbon peaks become very weak in intensity or become undiscernible when the sample is treated at 600 °C. The peaks at 37.1°, 43.2°, 62.7°, 75.28°, and 79.87° correspond to the (111), (200), (220), (311), and (222) planes of nickel oxide (JCPDS-780429), respectively. In NiO/C-4, NiO/C-5, and NiO/C-6, the peak positions at 44.35°, 51.7°, and 76.24° correspond to planes (111), (200), and (220) of carbon (JCPDS- 800017), respectively. Liu et al.[25] reported the formation of new crystalline carbon by laser ablation in liquid when no matching JCPDS data could be identified. The carbon coating on the NiO appears to be present in all three samples, but the content alone seem to decrease in the order of NiO/C-4 > NiO/C-5 > NiO/C-6, as evidenced by the decrease in intensity of the diffraction peaks corresponding to carbon (The elemental composition of the NiO/C was discussed in the EDS section). The crystallinity of NiO increases with an increase in calcination temperature. Debye−Scherrer formula was used to estimate the average grain size, it was founde to be 18, 21, and 22 nm for NiO/C-4, NiO/C-5 and NiO/C-6 samples.

Morphological Study and Possible Formation Mechanism. To evaluate the morphological features of the samples, FESEM of the samples have been studied. Figure 2 shows the

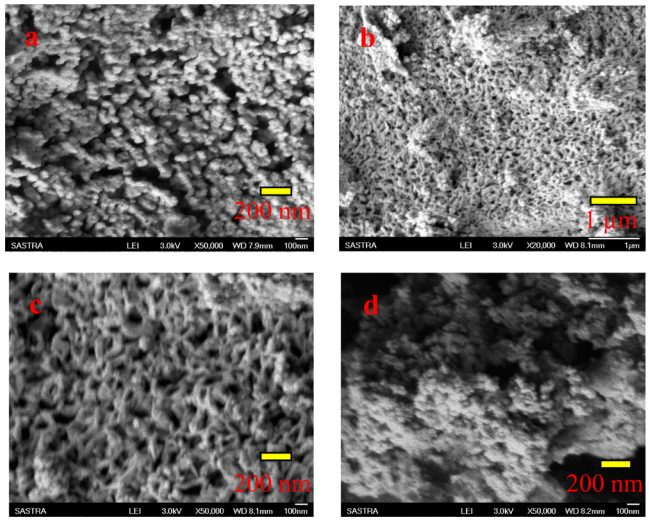

Figure 2. FESEM images of samples calcined at (a) 400 °C, (b, c) 500 °C, and (d) 600 °C.

FESEM images of the NiO/C-4, NiO/C-5, and NiO/C-6 samples. From the FESEM images, it is observed that the morphology depends on the calcinations temperature. FESEM of the sample calcined at 400 °C reveals formation of spherical particles with some uneven pores. These uneven pores are probably due to smaller quantities of carbon burn off. Samples calcined at 500 °C show a meshlike porous morphology of NiO/C due to the removal of carbon at a uniform rate. At an increased resolution, a meshlike network formation could be identified (Figure 2c). Figure 3 shows TEM images of the NiO/C-5 sample. From the TEM images, the porous nature of the NiO/C samples could be observed. The FESEM image of the sample calcined at 600 °C exhibits reduced porosity and even some degree of agglomeration of the network to form large clusters. Generally, increasing the calcination temperature damages the specific morphology.[26] The porous nature appears to be damaged at elevated calcination temperature. Figure 4 shows the EDS spectrum of the NiO/C-5 nanocomposites, and Figure S1 of the Supporting Information shows the EDS spectra of NiO/C-4 and NiO/C-6 nanocomposites. NiO/C-4, NiO/C-5, and NiO/C-6 samples reveal 13%, 9%, and 6% of

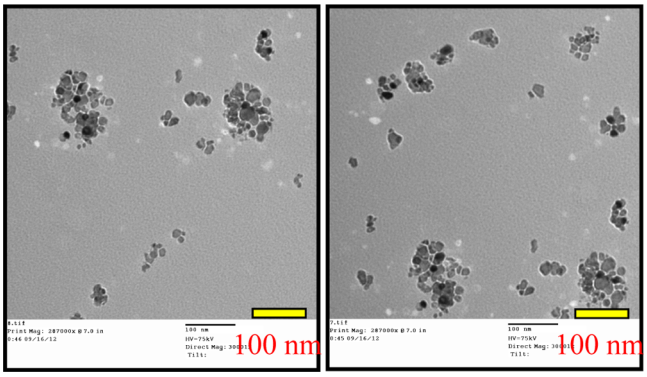

Figure 3. TEM images of NiO/C-5 sample.

carbon by weight, respectively. The Ni/O atom ratio from EDS analysis is close to unity confirming formation of NiO.

The formation of porous NiO/C is due to the simple precipitation of $Ni(OH)_2$ followed by the decomposition of carbonaceous material. The precipitation of $Ni(OH)_2$ occurs after the completion of various stages such as nucleation, coalescence, Ostwald-ripening, and self-aggregation. We have made an attempt to explain the formation of different morphologies in a pictorial manner. Scheme 1 shows the plausible mechanism for the formation of NiO/C nanocomposites. Initially, the nickel ions associate well with the starch matrix due to their high coordination with functional groups.[27] Dextrose acts as a chelating agent as well, while it enhances the diffusion and reaction rate.[28] The dextrose molecules interact with the starch molecules via hydrogen bonding. The interaction between nickel ions, starch, and dextrose molecules trigger supersaturation, thus providing nucleation sites for the growth of the $Ni(OH)_2$.[27] In the nucleation stage, the supersaturation is very high and electrostatic repulsive barriers are low due to the compression of the electric double layer between two particles, hence particles aggregate by weak Vander Waals interaction or electrostatic forces. Once nucleation occurs, the growth process starts due to the reduction of surface energy, i.e., decreasing the supersaturation. This growth process strongly depends on the material structure, properties of the solution, and nature of the

Scheme 1. Plausible Formation Mechanism of NiO/C Nanocomposites

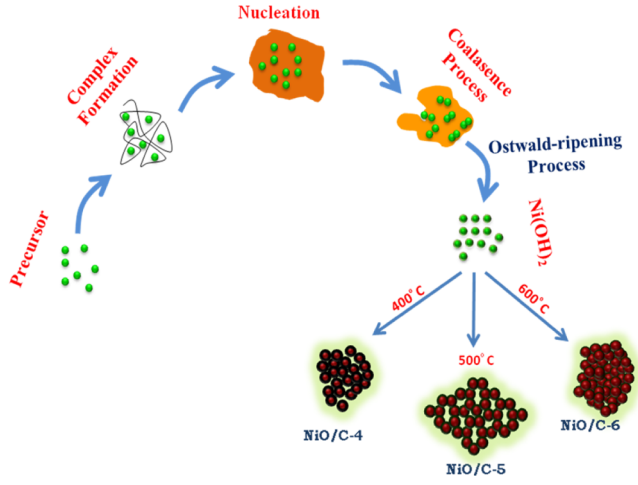

interface between particles.[29] In the growth process, first, two nanoparticles form a floc by weak Vander Waals interaction, and then the two nanoparticles cores coalesce. Because of continuous reaction process, the adjoining nanoparticles grow along particular crystal orientation due to the oriented attachment.[30,31] Then the pH decreases, and the growth by Ostwald-ripening starts.[31] Finally the $Ni(OH)_2$ powders settle due to rapid aggregation. The $Ni(OH)_2$ powders calcined at 400, 500, and 600 °C show variation in morphology. $Ni(OH)_2$ calcined at 400 °C shows some uneven pores due to initial burning of carbon. The samples calcined at 500 °C exhibit a highly porous nature due to burn off of carbon, but those at 600 °C do not show a porous structure due to collapse of the porous nature at higher temperatures.

The NiO/C-5 samples exhibit a porous nature; hence, the porous characteristics of these samples have been studied by the BET isotherm. Figure 5 shows the BET isotherm of the NiO/C-5 sample, and the inset shows the pore size distribution of the sample. According to the IUPAC classification, the isotherm can be classified as type IV. The NiO/C-5 sample exhibits a BET surface area of 33.19 $m^2 g^{-1}$. From the BJH pore size distribution, it is observed that the maxima peak centered

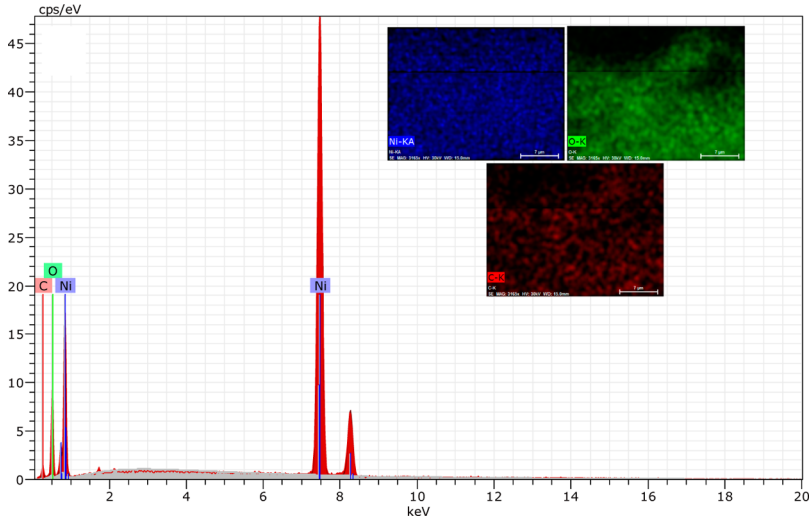

Figure 4. EDS spectrum of sample calcined at 500 °C. Inset shows elemental mapping of NiO/C-5.

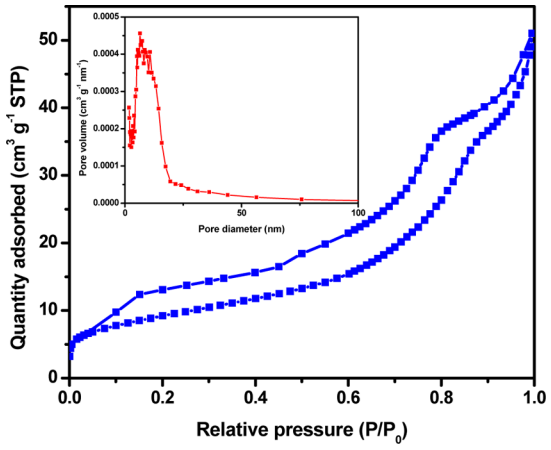

Figure 5. BET isotherm. Inset shows the pore size distribution curve.

at 6.4 nm. The average pore diameter was 10.3 nm. These results confirm the highly porous nature of NiO/C-5 samples. Thus, it is concluded that the porous nature is the cause for enhancing ion diffusion and the easy access of electrolyte ions into the electroactive surface.

Electrochemical Studies. The electrochemical properties strongly depend on the structure and morphology of the material.[32] Calcination temperature is one of the crucial factors for tuning the structure and morphology of the material. Hence, fixing the calcination temperature for superior electrochemical properties of the material is essential.[33] In order to get information on the supercapacitor performance of the prepared nanocomposite electrodes (NiO/C-4, NiO/C-5, and NiO/C-6), cyclic voltammetry, charge−discharge, and impedance analysis experiments have been performed.

Cyclic Voltametry. Cyclic voltammetry studies have been carried out for NiO/C electrodes calcined at different temperatures within the potential range from 0 to 0.5 V using 2.0 M KOH as the electrolyte. A nickel oxide electrode in alkaline solution stores charges in an electric double layer at the electrode/electrolyte interface and electrode surface through redox reactions.[34] Figure 6a−c shows the CV curve of NiO-4, NiO-5, and NiO-6 electrodes for different scan rates. CV curves that show well-defined redox peaks suggest the Faradic nature of the NiO rather than EDLC behavior. The asymmetrical nature of the anodic and respective cathodic peak is due to kinetic irreversibility of the redox process.[35] The charge storage of NiO electrodes arises from the following redox reaction.[35]

$$\mathrm{NiO} + z\mathrm{OH}^- \Leftrightarrow z\mathrm{NiOOH} + (1 - z)\mathrm{NiO} + ze^- \qquad (1)$$

The area under the curve of NiO/C-5 is higher than those of NiO/C-4 and NiO/C-6. The meshlike porous structure of

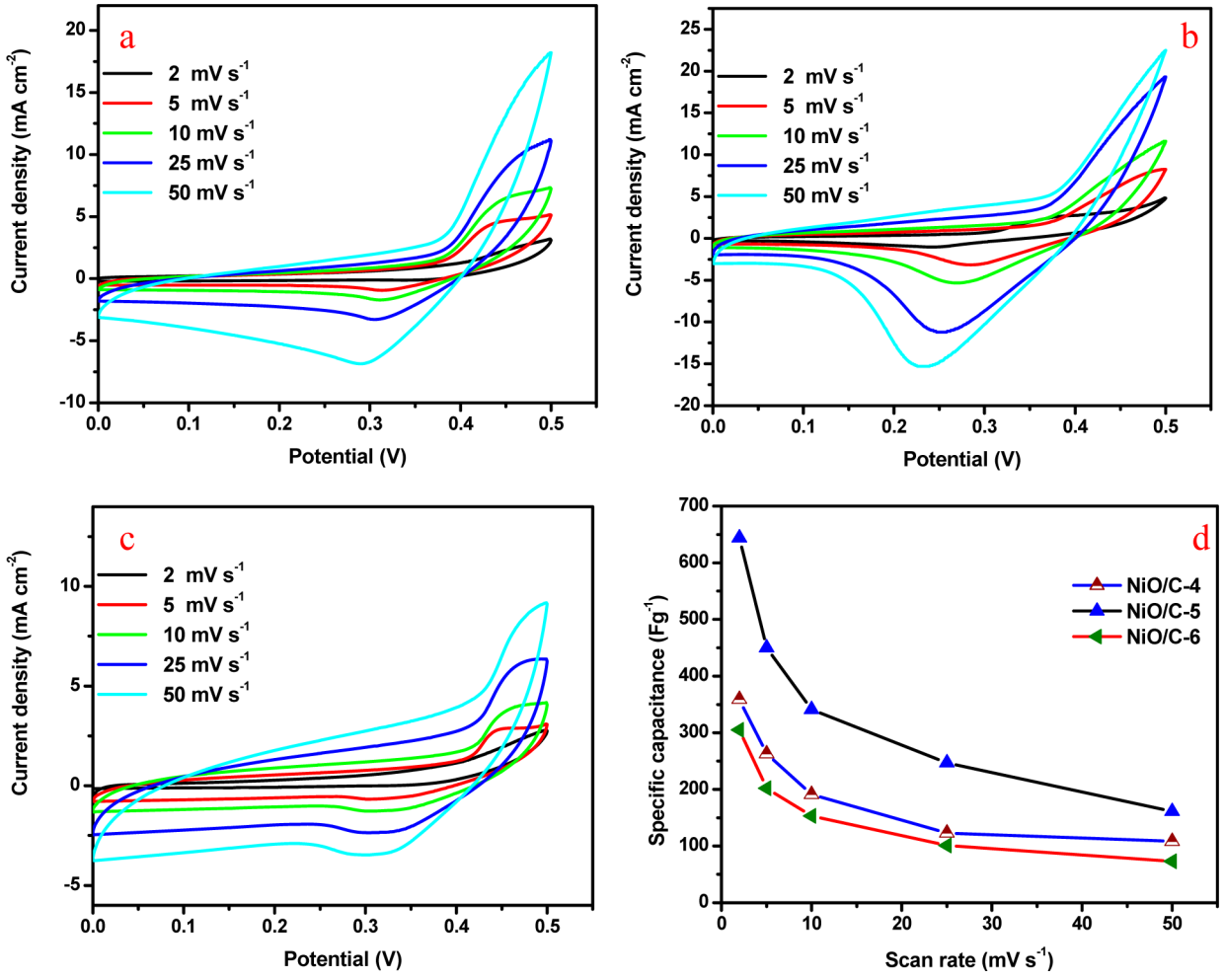

Figure 6. CV traces of (a) NiO/C-4, (b) NiO/C-5, and (c) NiO/C-6 electrodes at different scan rates. (d) Variation of specific capacitance as a function of scan rate.

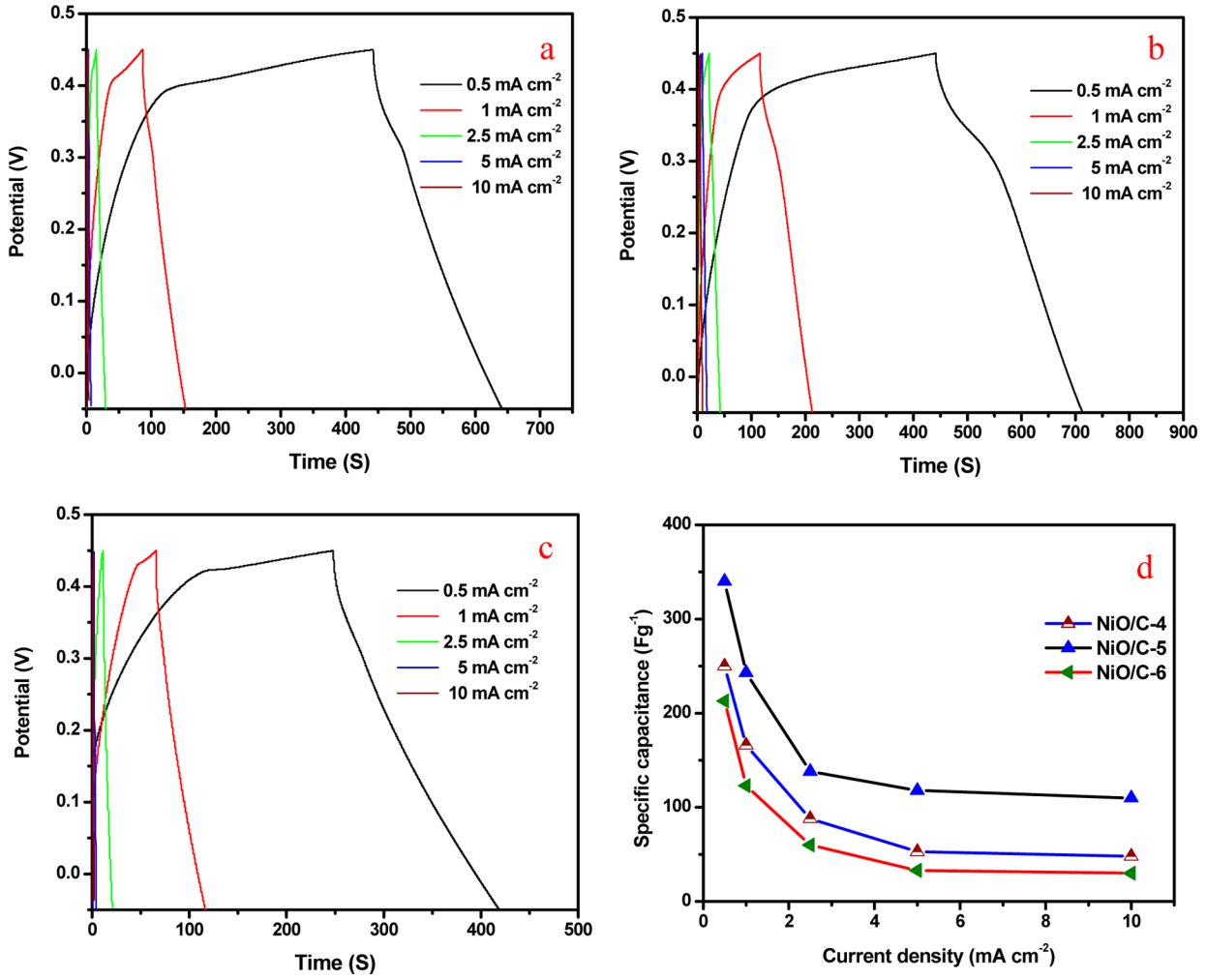

Figure 7. Charge−discharge curves of (a) NiO/C-4, (b) NiO/C-5, and (c) NiO/C-6 electrodes at different current densities. (d) Variation of specific capacitance as a function of current density.

NiO/C-5 facilitates the fast intercalation and deintercalation of the active species. Even though NiO/C-4 also has a porous structure, NiO/C-5 exhibits a larger area due to the highly porous nature, where as NiO/C-6 exhibits a smaller area due to poor morphological feature. The specific capacitance (C_s) values of NiO/C are obtained using the following equation.[36]

$$C_s = \frac{Q}{m\Delta V} \tag{2}$$

where, Q (C) is the average charge during anodic and cathodic scan, m (g) is the mass of the electrode, and ΔV (V) is the applied voltage window. The estimated specific capacitance values are 359, 644, and 305 F g^{-1} for NiO/C-4, NiO/C-5, and NiO/C-6 at a scan rate of 2 mV s^{-1}, respectively. The scan rate dependent specific capacitance is shown in Figure 6d. The specific capacitance values decrease with increasing scan rates. At high scan rates, the OH^- ions access the outer surface of the electrode, whereas at low scan rates, the OH^- ions intercalate well with the outer and inner pore surfaces. This low accessibility of OH^- ions resulted in a decrease in the specific capacitance value toward higher scan rates.[37] The carbon coating in the NiO/C composites leads to double layer capacitance; further, it also facilitates conducting pathways for ion transfer that contribute to increases in specific capacitance, in addition to suppressing aggregation of nickel oxide.[19,38]

Chronopotentiometry. To evaluate the cyclic behavior and stability of the NiO/C samples calcined at different temperatures, charge−discharge measurements were performed at different current densities from −0.05 to 0.45 V using 2.0 M KOH as the electrolyte. Figure 7a−c shows the charge−discharge curve of NiO/C-4, NiO/C-5, and NiO/C-6. A linear variation from −0.05 to ∼0.3 V indicates the EDLC behavior, and the sloped variation above ∼0.3 V indicates the pseudocapacitive nature of the NiO/C. The specific capacitance, C_s (Fg^{1-}) values were calculated using the following equation.[36]

$$C_s = \frac{i\Delta t}{m\Delta V} \tag{3}$$

where i (A) is discharge current, m (g) is the mass of the electrode, ΔV (V) is the potential drop during the discharge, and Δt (s) is the discharge time. The specific capacitance of NiO/C-4, NiO/C-5, and NiO/C-6 at a current density of 0.5 mA cm^{-2} is 250, 340, and 213 F g^{-1}, respectively. The porous structure of NiO/C-5 acts as a OH ion buffering reservoir that reduces the diffusion lengths for the electrolyte ions and ensures that enough electrolyte ions are in contact with larger surface of electroactive NiO/C electrode.[39] The charging and discharging curves at different current densities are not symmetrical due to kinetic irreversibility of the OH^- ions on

dx.doi.org/10.1021/sc400152r | ACS Sustainable Chem. Eng. 2013, 1, 1110−1118

the electrode.[24] Figure 7d shows the change in the specific capacitance value at different current densities for NiO/C-4, NiO/C-5, and NiO/C-6. The capacitance of the NiO/C electrodes decreases with increasing current densities. The voltage (IR) drop increases with increasing current density and decreases the specific capacitance of the electrode. At low current densities, the ions have enough time to intercalate and deintercalate; thus, the ions access the outer surface as well as the inner pores. But at high current densities, the ions access to only the outer surface of the electrode leads to a decrease in specific capacitance. The specific capacitance values of the NiO/C electrode from charge–discharge are lower than the cyclic voltametry results. This is due to a reduced ion access surface under higher current density. Because cyclic stability at higher current density is essential for practical application of supercapacitors, the NiO/C-5 electrodes were examined up to 1000 continuous charge–discharge cycles at a current density of 10 mA cm^{-2}. Figure 8 shows the profile of the specific capacitance values with number of cycles. From the stability curve, it is observed that the NiO/C-5 electrode has excellent cycling stability over 1000 cycles. Even after 1000 continuous charge–discharge cycles, the NiO/C-5 electrode retains 88% of the initial capacitance. Hence, the NiO/C-5 electrode is suitable material for supercapacitor application.

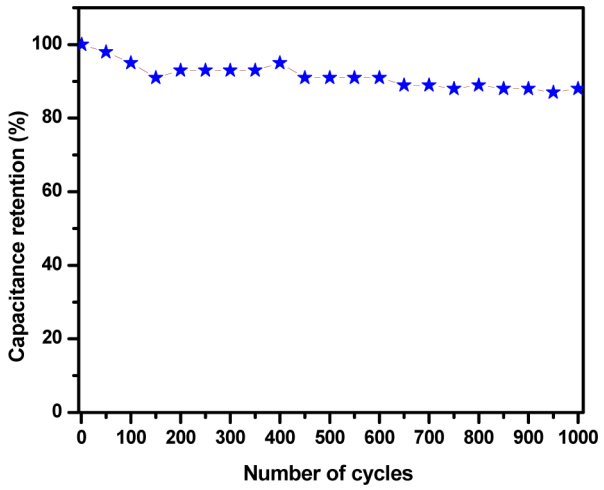

Figure 8. Cyclic stability charge–discharge curve of NiO/C-5 electrode at 10 mA cm^{-2}.

Electrochemical Impedance Spectroscopy. Electrochemically, it is preferred to have a low resistance for supercapacitors because they are power devices. The impedance plots of the NiO/C-5 electrode and NiO/C-4 and NiO/C-6 electrodes in the frequency range from 0.01 to 100 kHz at bias potential of 0.4 V are shown in Figure 9a and Figure S2a,b of the Supporting Information, respectively. The inset of Figure 9a shows the equivalent fitting circuit of NiO/C electrodes. R_s, R_{ct}, C_{dl}, and W are the solution resistance, charge-transfer resistance, double layer capacitance, and Warburg impedance. At high frequencies, the intercept on the real axis is solution resistance, which is 1.41, 2.66, and 1.39 Ω for NiO/C-4, NiO/C-5, and NiO/C-6 electrodes, respectively. This solution resistance is the combination of (i) ionic and electronic resistances, (ii) intrinsic resistance of the NiO/C electrode, and (iii) diffusive as well as contact resistance at the NiO/C electrode/current collector interface.[40] The semicircle at the high frequency region corresponds to the charge transfer resistance, R_{ct}. This charge transfer resistance is related to the electroactive surface area of the electrode due to the Faradic redox process of the NiO/C electrodes involving in the exchange of OH^- ions.[40]

The charge transfer resistance values are 1.09, 0.59, and 1.18 Ω for NiO/C-4, NiO/C-5, and NiO/C-6 electrodes, respectively. The lower R_{ct} value for NiO/C-5 is due to the enhanced diffusivity of the OH^- ions at the porous electrode.[17] The straight line portion at the low frequency region corresponds to the Warburg resistance, which is described as a diffusive resistance of the OH^- ions within the NiO/C electrodes. The specific capacitance values of the NiO/C electrodes were calculated from the impedance data using the following equation.[35,41]

$$C_s = \frac{1}{2\pi f Z''} \tag{4}$$

Figure 9b shows the frequency-dependent specific capacitance curve of NiO/C electrodes. The specific capacitance values for NiO/C-4, NiO/C-5, and NiO/C-6 electrodes are 331, 366, and 272 Fg^{1-}, respectively. These results are in good agreement with the cyclic voltammetric and charge–discharge results.

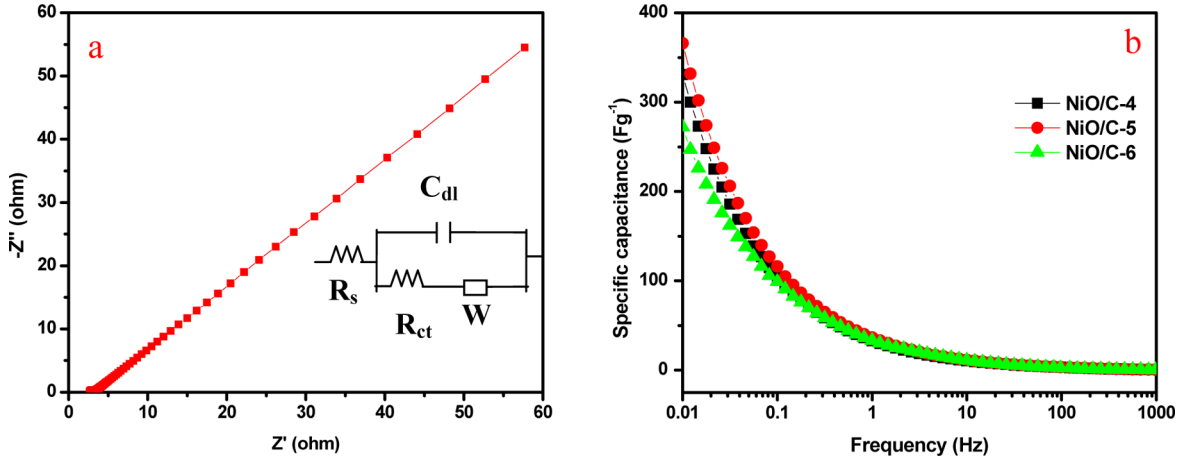

Figure 9. (a) Impedance plot of (a) NiO/C-5 electrode at 0.4 V. Inset shows the equivalent fitting circuit. (b) Frequency-dependent specific capacitance of NiO/C electrodes.

CONCLUSION

NiO/C nanocomposites were prepared at different calcination temperatures. NiO/C-5 shows a uniform porous structure. The NiO/C-5 electrode exhibits a maximum specific capacitance of 644 Fg^{1-} at 2 mV s^{-1}. The NiO/C-5 electrode has advantages over NiO/C-4 and NiO/C-6, as the uniform porous structure facilitates a larger number of active sites for ion access. The charge transfer resistance is low for NiO/C-5. This NiO/C-5 electrode exhibits high specific capacitance and low charge transfer resistance. Hence, NiO/C electrodes calcined at 500 °C are optimally suited for supercapacitor applications.

ASSOCIATED CONTENT

Supporting Information

EDS spectra of sample calcined at 400 and 600 °C and impedance plot of NiO/C-4 and NiO/C-6 electrodes. This material is available free of charge via the Internet at http://pubs.acs.org.

AUTHOR INFORMATION

Corresponding Author

*E-mail: muraligru@gmaill.com. Tel: +91 451 2452371. Fax: +91 451 2454466.

Notes

The authors declare no competing financial interest.

REFERENCES

(1) Lang, X.; Hirata, A.; Fujita, T.; Chen, M. Nanoporous metal/oxide hybrid electrodes for electrochemical supercapacitors. *Nat. Nanotechnol.* **2011**, *6*, 232−236.

(2) Lou, X. W.; Deng, D.; Lee, J. Y.; Feng, J.; Archer, L. A. Self supported formation of needlelike Co_3O_4 nanotubes and their application as lithium-ion battery electrodes. *Adv. Mater.* **2008**, *20*, 258−262.

(3) Chiu, H. C.; Yeh, C. S. Hydrothermal synthesis of SnO_2 nanoparticles and their gas-sensing of alcohol. *J. Phys. Chem. C* **2007**, *111*, 7256−7259.

(4) Huang, Z.; Natu, G.; Ji, Z.; Hasin, P.; Wu, Y. p-Type dye sensitized solar cells: A study by electrochemical impedance spectroscopy. *J. Phys. Chem. C.* **2011**, *115*, 25109−25114.

(5) Li, Y.; Zhao, X.; Zhang, Q.; Chen, D. Facile preparation and enhanced capacitance of the polyaniline/sodium alginate nanofiber network for supercapacitors. *Langmuir* **2011**, *27*, 6458−6463.

(6) Simon, P.; Gogotsi, Y. Materials for electrochemical capacitors. *Nat. Mater.* **2008**, *7*, 845−854.

(7) Hall, P. J.; Mirzaeian, M.; Fletcher, S. I.; Sillars, F. B.; Rennie, A. J. R.; Shitta-bey, G. O.; Wilson, G.; Cruden, A.; Carter, R. Energy storage in electrochemical capacitors: Designing functional materials to improve performance. *Energy Environ. Sci.* **2010**, *3*, 1238−1251.

(8) Zhao, X.; Sánchez, B. M.; Dobson, P. J.; Grant, P. S. The role of nanomaterials in redox-based supercapacitors for next generation energy storage devices. *Nanoscale* **2011**, *3*, 839−855.

(9) Shukla, A. K.; Sampath, S.; Vijayamohan, K. Electrochemical supercapacitors: Energy storage beyond batteries. *Curr. Sci.* **2000**, *79*, 1656−1661.

(10) Hu, C. C.; Chang, K. H.; Lin, M. C.; Wu, Y. T. Design and tailoring of the nanotubular arrayed architecture of hydrous RuO_2 for next generation supercapacitors. *Nano Lett.* **2006**, *6*, 2690−2695.

(11) Devaraj, S.; Munichandraiah, N. Effect of crystallographic structure of MnO_2 on its electrochemical capacitance properties. *J. Phys. Chem. C* **2008**, *112*, 4406−4417.

(12) Lang, J. W.; Kong, L. B.; Wu, W. J.; Luo, Y. C.; Kang, L. Facile approach to prepare loose-packed NiO nano-flakes materials for supercapacitors. *Chem. Commun.* **2008**, 4213−4215.

(13) Meher, S. K.; Rao, G. R. Ultralayered CO_3O_4 for high-performance supercapacitor applications. *J. Phys. Chem. C* **2011**, *115*, 15646−15654.

(14) Bao, S. J.; Li, C. M.; Guo, C. X.; Qiao, Y. Biomolecule-assisted synthesis of cobalt sulfide nanowires for application in supercapacitors. *J. Power Sources* **2008**, *180*, 676−681.

(15) Wang, K.; Huang, J.; Wei, Z. Conducting polyaniline nanowire arrays for high performance supercapacitors. *J. Phys. Chem. C* **2010**, *114*, 8062−8067.

(16) Li, J.; Zhao, W.; Huang, F.; Manivannan, A.; Wu, N. Single-crystalline $Ni(OH)_2$ and NiO nanoplatelet arrays as supercapacitor electrodes. *Nanoscale* **2011**, *3*, 5103−5109.

(17) Zhang, J.; Kong, L. B.; Cai, J. J.; Li, H.; Luo, Y. C.; Kang, L. Hierarchically porous nickel hydroxide/mesoporous carbon composite materials for electrochemical capacitors. *Microporous Mesoporous Mater.* **2010**, *132*, 154−162.

(18) Xia, X. H.; Tu, J. P.; Wang, X. L.; Gu, C. D.; Zhao, X. B. Hierarchically porous NiO film grown by chemical bath deposition via a colloidal crystal template as an electrochemical pseudocapacitor material. *J. Mater. Chem.* **2011**, *21*, 671−679.

(19) Fan, L.; Tang, L.; Gong, H.; Yao, Z.; Guo, R. Carbon-nanoparticles encapsulated in hollow nickel oxides for supercapacitor application. *J. Mater. Chem.* **2012**, *22*, 16376−16381.

(20) Huang, X. H.; Tu, J. P.; Zhang, C. Q.; Xiang, J. Y. Net-structred NiO-C nanocomposite as Li-Intercalation electrode material. *Electrochem. Commun.* **2007**, *9*, 1180−1184.

(21) Liu, X. M.; Zhang, X. G.; Fu, S. Y. Preparation of urchinlike NiO nanostructures and their electrochemical capacitive behaviors. *Mater. Res. Bull.* **2006**, *41*, 620−627.

(22) Fu, G. R.; Hu, Z. A.; Xie, L. J.; Jin, X. Q.; Xie, Y. L.; Wang, Y. X.; Zhang, Z. Y.; Yang, Y. Y.; Wu, H. Y. Electrodepositon of nickel hydroxide films on nickel foil and its electrochemical performances for supercapacitor. *Int. J. Electrochem. Sci* **2009**, *4*, 1052−1062.

(23) Srinivasan, V.; Weidner, J. W. Studies on the capacitance of nickel oxide films: Effect of heating temperature and electrolyte concentration. *J. Electrochem. Soc.* **2000**, *147*, 880−885.

(24) Meher, S. K.; Rao, G. R. Microwave-mediated synthesis for improved morphology and pseudocapacitance performance of nickel oxide. *ACS Appl. Mater. Interfaces* **2011**, *3*, 2063−2073.

(25) Liu, P.; Cao, Y. L.; Wang, C. X.; Chen, X. Y.; Yang, G. W. Micro-and nanocubes of carbon with C_8-like and blue lumincescence. *Nano Lett.* **2008**, *8*, 2570−2575.

(26) Lee, J. W.; Ahn, T.; Kim, J. H.; Ko, J. M.; Kim, J. D. Nanosheets based mesoporous NiO microspherical structures via facile and template-free method for high performance supercapacitors. *Electrochim. Acta* **2011**, *56*, 4849−4857.

(27) Chen, Y.; Cao, J.; Zheng, M.; Ke, X.; Ji, H.; Liu, J.; Ji, G. Novel synthesis of nanoporous nickel oxide and nickel nanoparticles/amorphous carbon composites using soluble starch as the template. *Chem. Lett.* **2006**, *35*, 700−701.

(28) Zhang, Y. C.; Xing, R.; Hu, X. Y. A green hydrothermal route to copper nanocrystallites. *J. Cryst. Growth* **2004**, *273*, 280−284.

(29) Soare, L. C.; Bowen, P.; Lemaitre, J.; Holfmann, H. Precipitation of nanostructured copper oxalate: substructure and growth mechanism. *J. Phys. Chem. B.* **2006**, *110*, 17763−17771.

(30) Mullaugh, K. M.; Luther, G. W., III Growth kinetics and long-term stability of CdS nanoparticles in aqueous solution under ambient conditions. *J. Nanopart. Res.* **2011**, *13*, 393−404.

(31) Yuan, C.; Zhang, X.; Su, L.; Gao, B.; Shen, L. Facile synthesis and self-assembly of hierarchical porous NiO nano/micro spherical superstructures for high performance supercapacitors. *J. Mater. Chem* **2009**, *19*, 5772−5777.

(32) Zhang, X.; Shi, W.; Zhu, J.; Zhao, W.; Ma, J.; Mhaisalkar, S.; Maria, T. L.; Yang, Y.; Zhang, H.; Hng, H. H.; Yan, Q. Synthesis of porous NiO nanocrystals with controllable surface area and their application as supercapacitor electodes. *Nano Res.* **2010**, *3*, 643−652.

(33) Sun, X.; Wang, G.; Hwang, J. Y.; Lian, J. Porous nickel oxide nano-sheets for high performance pseudocapacitance materials. *J. Mater. Chem.* **2011**, *21*, 16581−16588.

(34) Xiong, S.; Yuan, C.; Zhang, X.; Qian, Y. Mesoporous NiO with various hierarchical nanostructures by quasi-nanotubes/nanowires/nanorods self-assembly: controllable preparation and application in supercapacitors. *CrystEngComm* **2011**, *13*, 626−632.
(35) Meher, S. K.; Justin, P.; Rao, G. R. Nanoscale morphology dependent pseudocapacitance of NiO: Influence of intercalating anions during synthesis. *Nanoscale* **2011**, *3*, 683−692.
(36) Yan, J.; Khoo, E.; Sumboja, A.; Lee, P. S. Facile coating of manganese oxide on tin oxide nanowires with high-performance capacitive behavior. *ACS Nano* **2010**, *4*, 4247−4255.
(37) Patil, U. M.; Gurav, K. V.; Fulari, V. J.; Lokhande, C. D.; Joo, O. S. Characterization of honeycomb-like "α-Ni$(OH)_2$" thin films synthesized by chemical bath deposition method and their supercapacitor application. *J. Power Sources* **2009**, *188*, 338−342.
(38) Nagamuthu, S.; Vijayakumar, S.; Muralidharan, G. Synthesis of Mn_3O_4/amorphous carbon nanoparticles as electrode material for high performance supercapacitor applications. *Energy Fuels* **2013**, DOI: 10.1021/ef400212b.
(39) Wang, D. W.; Li, F.; Liu, M.; Lu, G. Q.; Cheng, H. M. 3D aperiodic hierarchical porous graphitic carbon material for high-rate electrochemical capacitive energy storage. *Angew. Chem., Int. Ed* **2008**, *47*, 373−376.
(40) Wu, M. S.; Hsieh, H. H. Nickel oxide/hydroxide nanoplatelets synthesized by chemical precipitation for electrochemical capacitors. *Electrochim. Acta* **2008**, *53*, 3427−3435.
(41) Conway, B. E. *Electrochemical Supercapacitors: Scientific Fundamentals and Technological applications*; Kluwer Academic/Plenum Publishers: New York, 1999.